



Article

Structural Insights into β -arrestin/CB1 Receptor Interaction: NMR and CD Studies on Model Peptides

Paula Morales ^{1,2,*} , Marta Bruix ¹ and M. Angeles Jiménez ^{1,*}

¹ Departamento de Química Física Biológica, Instituto de Química Física Rocasolano (IQFR-CSIC), Serrano 119, 28006 Madrid, Spain; marta.bruix@gmail.com

² Instituto de Química Médica (IQM-CSIC), Juan de la Cierva 3, 28006 Madrid, Spain

* Correspondence: paula.morales@iqm.csic.es (P.M.); majimenez@iqfr.csic.es (M.A.J.)

Received: 15 September 2020; Accepted: 28 October 2020; Published: 30 October 2020



Abstract: Activation of the cannabinoid CB1 receptor induces different cellular signaling cascades through coupling to different effector proteins (G-proteins and β -arrestins), triggering numerous therapeutic effects. Conformational changes and rearrangements at the intracellular domain of this GPCR receptor that accompany ligand binding dictate the signaling pathways. The GPCR-binding interface for G proteins has been extensively studied, whereas β -arrestin/GPCR complexes are still poorly understood. To gain knowledge in this direction, we designed peptides that mimic the motifs involved in the putative interacting region: β -arrestin1 finger loop and the transmembrane helix 7-helix 8 (TMH7-H8) elbow located at the intracellular side of the CB1 receptor. According to circular dichroism and NMR data, these peptides form a native-like, helical conformation and interact with each other in aqueous solution, in the presence of trifluoroethanol, and using zwitterionic detergent micelles as membrane mimics. These results increase our understanding of the binding mode of β -arrestin and CB1 receptor and validate minimalist approaches to structurally comprehend complex protein systems.

Keywords: CB1; β -arrestin1; NMR; Circular dichroism; GPCR

1. Introduction

The therapeutic effects of cannabinoids have long been known; however, it was not until a few decades ago that their mechanism of action was elucidated. In the late 1980s, receptors targeted by phytocannabinoids were identified in rat brain [1]. Subsequent cloning of this G protein-coupled receptor (GPCR) consolidated the discovery of the first cannabinoid receptor, CB1 [2].

CB1 is highly expressed throughout the central nervous system, being one of the most abundant GPCRs in the human brain [3]. CB1 receptors are also found in the peripheral nervous system, as well as in other organs and tissues including endocrine glands, spleen, heart or the gastrointestinal tract. This expression pattern confers upon CB1 a relevant role in the modulation of numerous physiopathological processes including memory processing, pain regulation or neurodegeneration [3–6]. A growing body of research supports the notion that CB1 represents a promising target for the development of novel drugs for the treatment of diverse pathologies including neurodegenerative, cancer or metabolic disorders [7–15].

The activation of this receptor involves complex signaling pathways whose mechanisms still need to be fully unraveled. CB1 receptors are mainly coupled to $G_{\alpha i/o}$ proteins, negatively to adenylyl cyclase (AC) and positively to mitogen-activated protein kinases (MAPK). Other G_{α} isoforms, such as $G_{\alpha s}$ [16–20], and $G_{\alpha q/11}$ [21], have also been shown to couple to CB1 under particular

circumstances. Upon CB1-mediated $G_{\alpha i/o}$ coupling, AC is inhibited, thus inhibiting the conversion of ATP to cyclic AMP (cAMP). CB1 activation also triggers increased phosphorylation of extracellular signal-regulated kinase 1/2 (pERK1/2). The $G_{\beta\gamma}$ subunits, dissociated from the $G_{\alpha i/o}$, activate G protein-coupled inwardly rectifying potassium channels (GIRKs) and phosphatidylinositol-3-kinase (PI3K) and inhibit voltage-gated calcium channels (VGCC) [22,23]. Moreover, upon G protein activation, G protein-coupled receptor kinases (GRKs) phosphorylate specific serines and threonines in the intracellular domain of the receptor, inducing β -arrestin recruitment [24]. Two β -arrestin isoforms have been shown to be recruited to CB1: β -arrestin1, which triggers the activation of the ERK pathway, and β -arrestin2, which leads to receptor desensitization and internalization [25–27].

In addition to the G-protein canonical pathway, G-protein independent β -arrestin recruitment to GPCRs was recently demonstrated in diverse GPCRs [28–31]. Most known CB1 agonists activate the receptor through both G protein and β -arrestin signaling pathways in an unbiased manner [32–34]. The search of biased ligands has greatly increased in the last years in the cannabinoid field [27,35,36]. These functionally selective ligands should be able to stabilize distinct GPCR states that vary the ability of the receptor to activate specific transducers, such as activation of different G-proteins and/or signaling through β -arrestins, leading to different physiologic outcomes [37–40]. This may provide optimized therapeutic results while avoiding undesired effects mediated through specific pathways. However, the design of biased ligands remains a challenge, since the precise nature of conformational receptor changes inducing pathway specificity has not yet been unraveled.

From a structural perspective, the G-protein activation mechanism of GPCRs has been extensively studied [41–45]. However, GPCR conformational changes that result in β -arrestin coupling have not yet been fully explained. High-resolution crystal structures of the CB1 receptor, in its G-protein inactive and active states, have been recently reported [46–48]. Moreover, cryoelectron microscopy structures of CB1- G_i complexes bound to potent agonists were recently resolved, providing insights into the G-protein coupling activation mechanism of CB1 [49,50]. Nevertheless, no CB1 receptor structure in complex with β -arrestin has been determined to date.

In an effort to better understand the β -arrestin1/CB1 receptor interface, we designed peptides that mimic the motifs potentially involved in the interacting region. Circular dichroism (CD) and nuclear magnetic resonance (NMR) studies were performed to help to determine the conformation of these peptides and characterizing the key structural features of their interaction.

2. Results and Discussion

2.1. Peptide Design

Since no experimental structure of the CB1/ β -arrestin complex has been reported to date, the design of peptides that mimic the interacting motifs in the CB1/ β -arrestin1 complex was based on previously reported data on GPCR/arrestin interface. To illustrate the region of interest, we developed a model (Figure 1) using as templates the crystal structures of CB1 receptors in their active state (PDB 5XRA) and the rhodopsin/arrestin complex (PDB 5W0P), which was the only GPCR/arrestin complex available at the beginning of this work. In the three GPCR/ β -arrestin complexes reported this year, the interacting regions are analogous, although the β -arrestin finger loop displays structural diversity [51–53].

Concerning β -arrestin1, it has been reported that its finger loop region (FL, Figure 1) is a critical determinant of arrestin coupling to GPCRs [51–56]. The finger loop region was first identified by sequence alignment of several β -arrestins (Supplementary Table S1). Then, the potential effects of including the preceding and following residues on helical tendency and solubility was examined by the AGADIR and ProtParam web servers [57,58]. The sequence for the β -arrestin1 model peptide was selected as the shortest sequence having the highest helical tendency and being the most soluble at the neutral (or slightly acidic) pH values used in the NMR study (note that peptide solubility is usually minimal at the isoelectric point, pI; Supplementary Table S1). This β -arrestin1 model peptide

(β -arr1⁶³⁻⁷⁶) includes the preceding residue and three after the finger loop motif, as indicated in Figure 1. The β -arrestin finger loop is structurally diverse in the reported GPCR/ β -arrestin complexes, adding interest to study the structure of this region by itself.

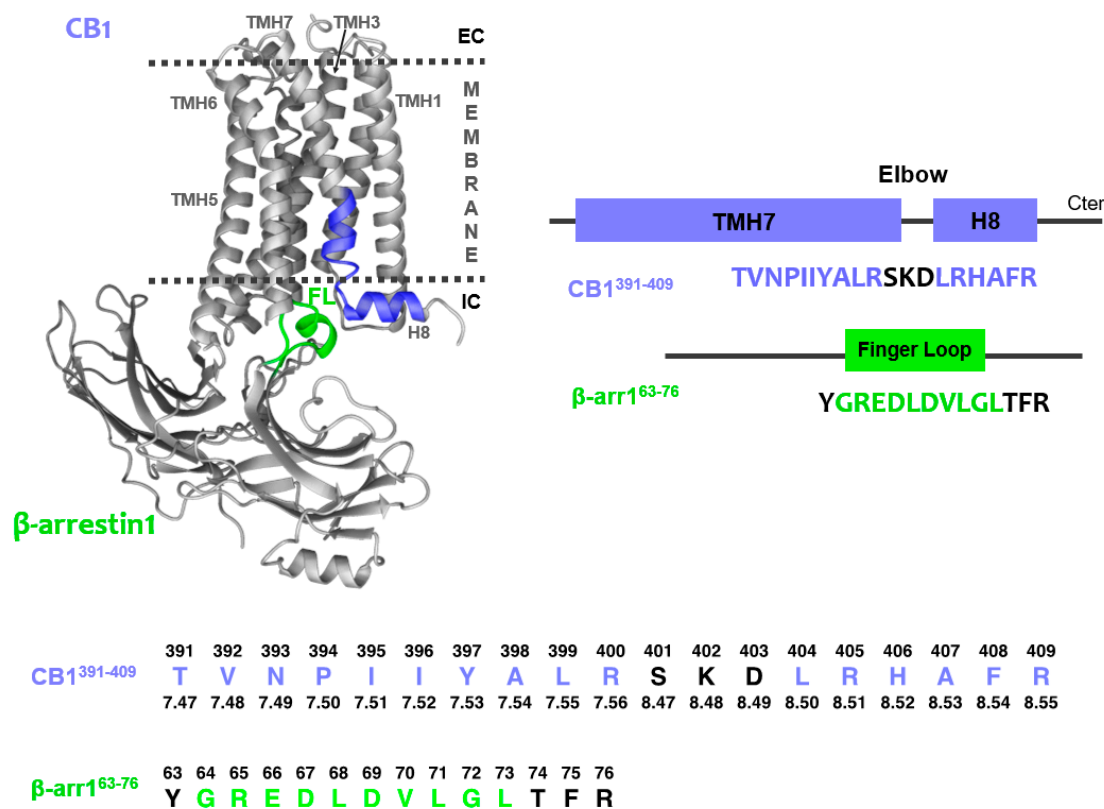


Figure 1. CB1/ β -arrestin1 complex model [templates: PDB 5XRA (CB1 receptor active state crystal structure) and 5W0P (Rho/ β -arrestin complex)]. The CB1/ β -arrestin1 interface to be studied is colored (green: β -arr1⁶³⁻⁷⁶; blue: CB1³⁹¹⁻⁴⁰⁹) while other domains in the GPCR and the scaffolding protein are represented in grey. Note that β -arrestin finger loop (FL) is not helical in other reported GPCR/ β -arrestin complexes [51–53]. At the bottom, the absolute sequence numbers are shown above the peptide sequences; in the case of CB1³⁹¹⁻⁴⁰⁹ the Ballesteros and Weinstein numbering of GPCRs is indicated below the sequence.

As shown in this figure, the general topology of GPCRs encompasses seven transmembrane helices (TMH) connected by intracellular and extracellular loops and a short cytoplasmic helical domain (H8) extending from TMH7. This helical segment is oriented in parallel to the membrane surface and perpendicularly to the TMH bundle.

The scarce structural knowledge available on GPCR/arrestin complexes indicates, as seen in the model of CB1/ β -arrestin1 (Figure 1), that the β -arrestin1 finger loop may be inserted into the bundle intracellularly close to the TMH7-H8 elbow area [51,52,55,59]. Therefore, the sequence for the CB1 peptide encompasses the TMH7-H8 region, located at the intracellular side of the CB1 receptor. As in the case of β -arr1⁶³⁻⁷⁶, the specific peptide sequence (CB1³⁹¹⁻⁴⁰⁹; Figure 1) was selected as the shortest peptide with higher α -helical propensity and solubility upon analysis using the AGADIR and protparam webserver [57,58] (Supplementary Table S2).

To avoid effects of the ionisable amino and carboxylate groups, the N- and C-termini of the two peptides were acetylated and amidated, respectively.

2.2. Structural Behavior of the Free CB1 and β -Arrestin1 Peptides

The conformation of the TMH7-H8 CB1 and β -arrestin1 peptides independently was examined in aqueous solution, in the presence of 30% of trifluoroethanol (TFE), a secondary structure enhancer [60], and using zwitterionic detergent micelles (dodecylphosphocholine, DPC) as membrane mimics.

We firstly characterized the structural behavior of the two peptides using circular dichroism (CD). As depicted in Figure 2, the CD spectra of the two peptides in water solution showed a minimum at about 197 nm, which indicated that they were mainly random coils, whereas they tended to form helical conformations in the presence of TFE or DPC micelles, as shown by the observed maximum below 195 nm and the minima at 208 nm and 222 nm. The helix percentages estimated from the ellipticity at 222 nm ($[\theta]^{222\text{nm}}$) are given in Table 1.

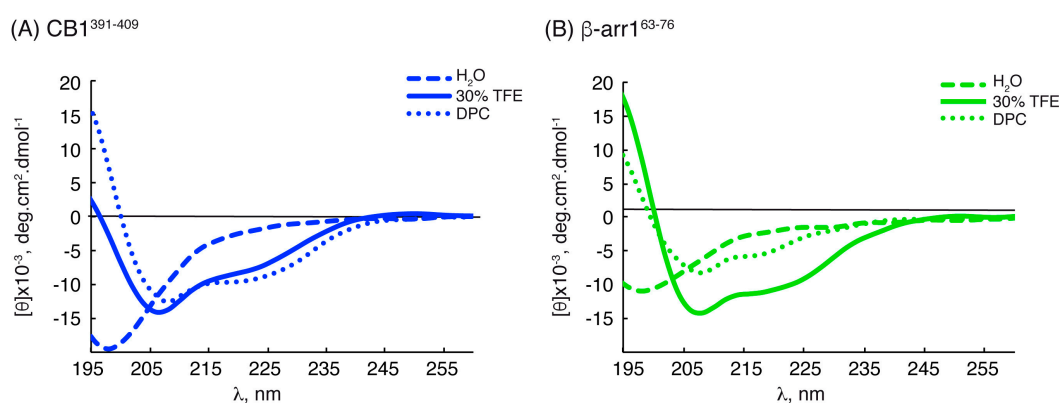


Figure 2. CD spectra of CB1³⁹¹⁻⁴⁰⁹ (A) and β -arr1⁶³⁻⁷⁶ (B) in H₂O (dashed line), TFE (continuous line) and DPC (dotted line) (30 mM). Data were collected at 5 °C, pH 5.5 and 50 μ M peptide concentration.

Table 1. Percentages of helical populations for CB1³⁹¹⁻⁴⁰⁹ and β -arr1⁶³⁻⁷⁶ peptides from CD and NMR data (see Materials & Methods) in H₂O, TFE and DPC at 25 °C.

Peptide	Conditions	$[\theta]^{222\text{nm}}$, deg.cm ² .dmol ⁻¹	% Helix ^[a] from $[\theta]^{222\text{nm}}$	Helix Length	Av. $\Delta\delta_{\text{H}\alpha}$, ppm	% α -Helix from $\Delta\delta_{\text{H}\alpha}$	Av. $\Delta\delta_{\text{C}\alpha}$, ppm	% α -Helix from $\Delta\delta_{\text{C}\alpha}$	Av. % Helix ^[c]
CB1 ³⁹¹⁻⁴⁰⁹	H ₂ O	-2178.68	13	P394-K402	-0.09 ^[b]	22 ^[b]	+0.48 ^[b]	16 ^[b]	19 \pm 3 ^[b]
				L404-F408	-0.07 ^[b]	18 ^[b]	+0.33 ^[b]	11 ^[b]	14 \pm 4 ^[b]
	TFE	-7931.79	28	P394-K402	-0.24	62	+2.50	81	71 \pm 9
				L404-F408	-0.14	37	+1.52	49	43 \pm 6
	DPC	-9415.07	32	P394-K402	-0.25	64	+2.01	65	64 \pm 1
				L404-F408	-0.23	58	+1.69	54	56 \pm 2
β -arr1 ⁶³⁻⁷⁶	H ₂ O	-1750.71	12	E66-T74	-0.06 ^[b]	16 ^[b]	+0.56 ^[b]	18 ^[b]	17 \pm 2 ^[b]
	TFE	-10229.3	34	E66-T74	-0.12	31	+1.79	58	45 \pm 13
	DPC	-3626.36	17	R65-T74	-0.13	34	+1.22	39	37 \pm 3

^[a] Notice that CD-estimated helix percentages are an average for all the peptide residues, whereas NMR-estimated helix percentages are for the residues within the helix. ^[b] Values measured at 5 °C. ^[c] Reported errors are standard deviations for the mean of the percentages obtained from the $\Delta\delta_{\text{H}\alpha}$ and $\Delta\delta_{\text{C}\alpha}$ values.

To gain further structural information, the peptides were characterized using NMR. The NMR spectra of the two peptides were fully assigned in the three experimental conditions, i.e., aqueous solution, in the presence of TFE and in DPC micelles (chemical shifts are reported in the supplementary material: Tables S3–S8).

Most residues of the two peptides show negative $\Delta\delta_{\text{H}\alpha}$ and positive $\Delta\delta_{\text{C}\alpha}$ values (Figure 3 and Figure S3), which are large in magnitude in TFE and DPC micelles, and small in aqueous solution. In agreement with the CD data, this indicates that the peptides form helical structures in TFE and DPC, and have only a low helical tendency in aqueous solution. A detailed examination of the profiles showed that CB1³⁹¹⁻⁴⁰⁹ presents two helical regions (P394-K402 and L404-F408), separated by the

residue D403, which showed positive $\Delta\delta_{H\alpha}$ values in TFE and DPC (Figure 3), and negative $\Delta\delta_{C\alpha}$ values in aqueous solution and in DPC (Figure S3). The helical region in the β -arr1⁶³⁻⁷⁶ peptide extends from E66 to T74 in aqueous solution and in TFE, and from R65 to T74 in DPC. The percentages of helical populations estimated from $\Delta\delta_{H\alpha}$ and $\Delta\delta_{C\alpha}$ are given in Table 1.

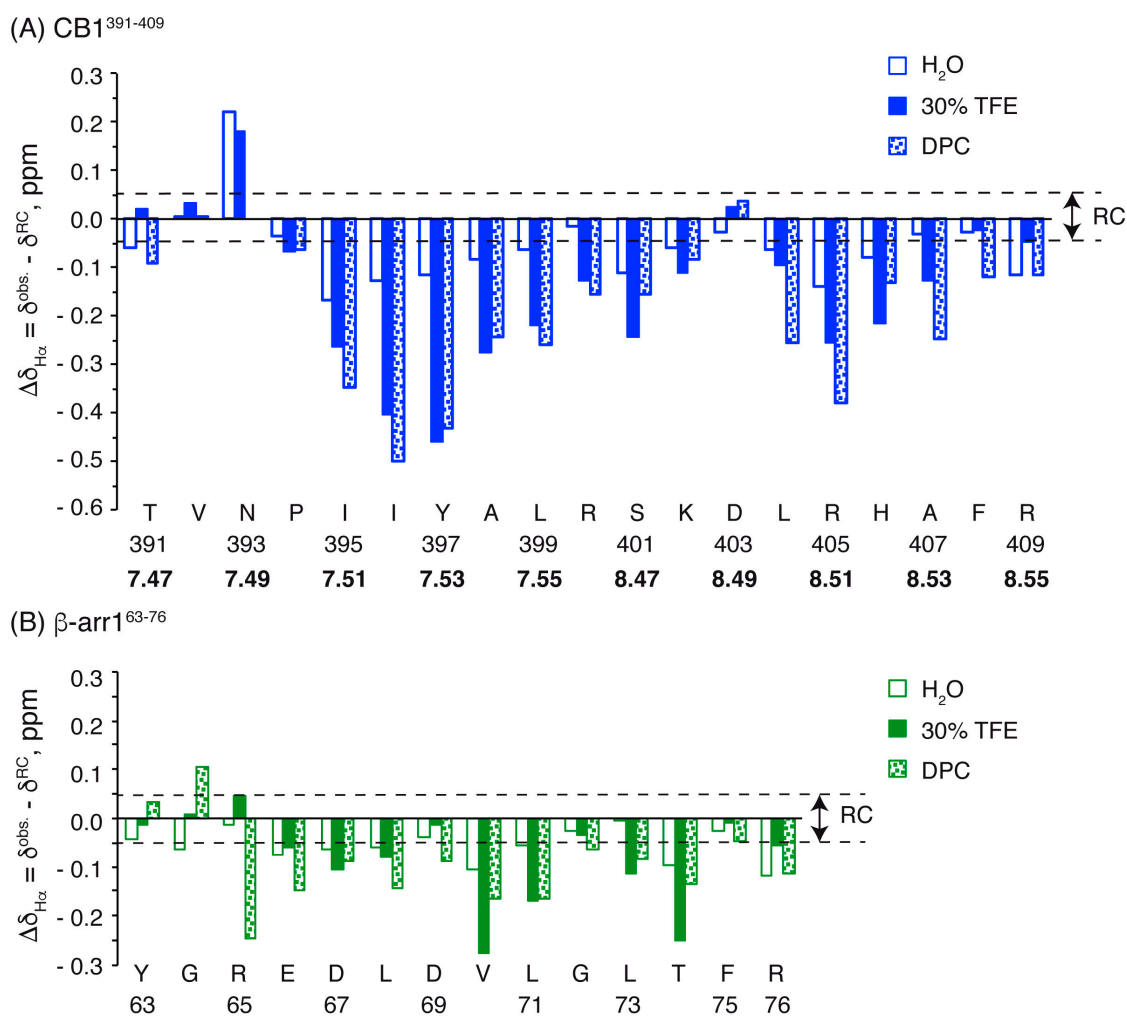


Figure 3. $\Delta\delta_{H\alpha}$ values plotted as a function of residue number for CB1³⁹¹⁻⁴⁰⁹ (A) and β -arr1⁶³⁻⁷⁶ (B) in H₂O (open bars), TFE (filled bars) and DPC (dotted bars) (30 mM). In all cases pH 5.5 and 25 °C. Dashed lines indicate the random coil (RC) range ($|\Delta\delta_{H\alpha}| \leq 0.05$ ppm). In the case of CB1³⁹¹⁻⁴⁰⁹, the Ballesteros and Weinstein numbering is shown in bold.

Further evidence about the helix formation in the two peptides came from the sets of NOEs present in TFE and DPC, which included those characteristic of helical structures, i.e., sequential NN(i,i+1), and the nonsequential α N(i,i+3), and $\alpha\beta$ (i,i+3). Examples of these NOEs are shown in the Supplementary Figures S1 and S2.

The preferred structures of the two peptides were calculated on the basis of distance and angle restraints derived, respectively, from the NOEs and the chemical shifts measured in TFE and in DPC and using the program CYANA (see Materials and Methods). The quality of the resulting structures is good (see Ramachandran plots at Supplementary Figure S4) and they are well defined (see RMSD values in Table S12). Figures 4 and 5 illustrate overlays of the 20 lowest target function conformers for CB1³⁹¹⁻⁴⁰⁹ and β -arr1⁶³⁻⁷⁶ peptides, as well as a representative conformer of the ensemble. In agreement with the qualitative analysis of $\Delta\delta_{H\alpha}$ and $\Delta\delta_{C\alpha}$ profiles, CB1³⁹¹⁻⁴⁰⁹ in both TFE and DPC exhibits two

helical regions, i.e., a long helix extending residues P394 to K402 and a short one spanning residues L404 to F408 (Figures 3A and 4). The angle between the two helical regions shows certain variability among the conformers within the structural ensembles, but they are approximately perpendicular each other ($94^\circ \pm 15^\circ$ in TFE; $75^\circ \pm 30^\circ$ in DPC; Figure 4) as in the crystalline structure of free CB1 (97° in PDB ID: 5XRA). TMH7, which ends at residue L399 in crystalline full-length CB1 receptor, extends up to residue K402 in the CB1³⁹¹⁻⁴⁰⁹ peptide both in TFE and in DPC. This result is in agreement with the previously reported structure for another CB1-derived peptide containing the same region [61]. Tyukhtenko and coworkers studied the structure of the TMH7-H8 span (CB1³⁷⁷⁻⁴¹⁶) obtaining a lengthy hydrophobic α -helical segment and a short amphipathic α -helix (H8) orthogonally oriented to TMH7.

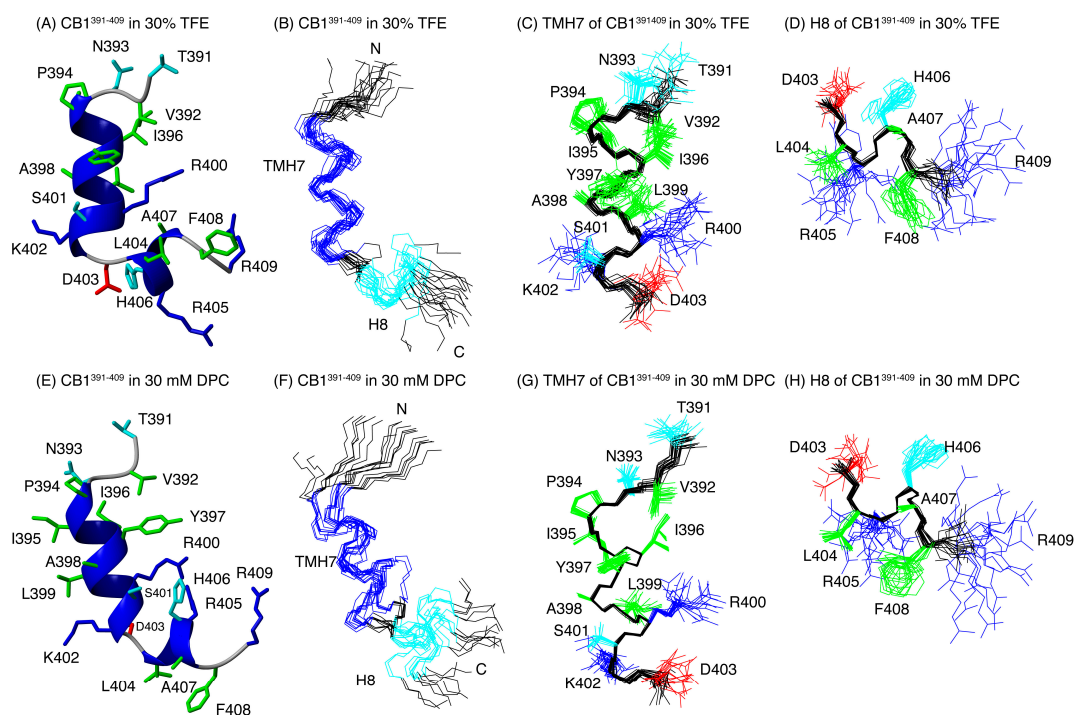


Figure 4. CB1³⁹¹⁻⁴⁰⁹ structure in 30% TFE (A–D) and in DPC micelles (E–H). Ribbon representation of the lowest target conformer of the structural ensemble (A,E). Overlay of the backbone atoms of the 20 lowest target function conformers (B,F). Overlay of residues 394–402 (helix TMH7; panels (C,G)) Overlay of residues 403–407 (helix H8; panels (D,H)). In panels (A–E), the backbone atoms of helices TMH7 and H8 are coloured in blue. The side-chains are shown in panels (F–H). The aliphatic and aromatic side chains are displayed in green, the Glu and Asp side chains in red, the Arg and Lys side chains in blue, and the Asn, His, Thr, and Ser side chains in cyan.

Our structural studies demonstrated that the β -arr1⁶³⁻⁷⁶ peptide also formed helical conformations in DPC and TFE (Figure 5). In agreement with our observations, various studies have indicated that in its activated state, the β -arrestin finger loop adopts helical conformations [55,56,62]. However, it is important to note that conformational plasticity of the finger loop was observed in previously reported GPCR/arrestin complexes [51–55]. While in the rhodopsin/arrestin complexes the finger loop forms a helical domain [54,55], in the recently solved muscarinic 2 receptor/arrestin complex [53], the finger loop adopts an extended loop configuration. This suggests that it can be ordered in different conformations or adopt diverse relative orientations in order to enable the recognition of a wide variety of GPCRs.

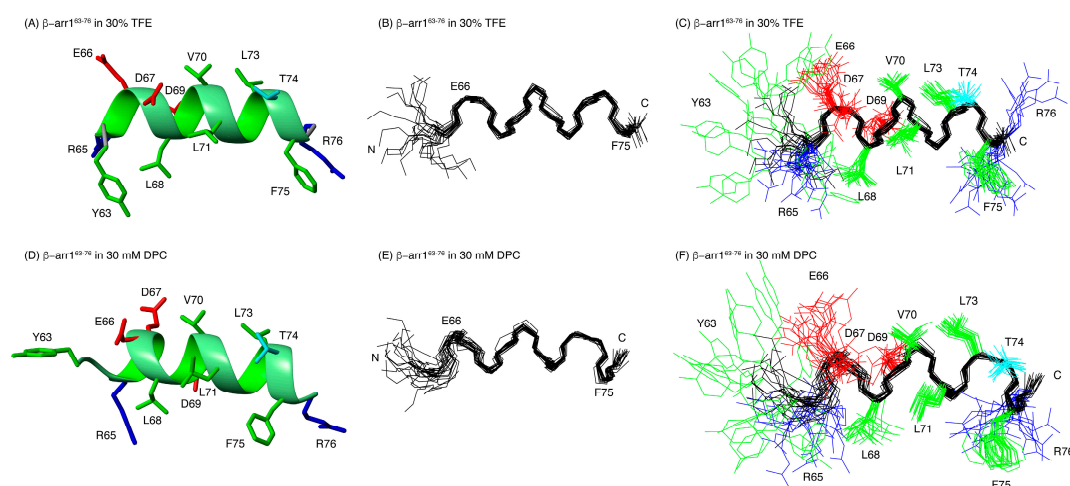


Figure 5. NMR structure of β -arr1⁶³⁻⁷⁶ in 30 % TFE (A–C) and in DPC micelles (D–F). Ribbon representation of the lowest target conformer of the structural ensemble (A,D). Overlay of the backbone atoms of the 20 lowest target function conformers (B,E). The side-chains are shown in panels (A,C–E). The aliphatic and aromatic side chains are displayed in green, the Glu and Asp side chains in red, the Arg and Lys side chains in blue, and the Thr side chains in cyan.

2.3. Characterization of the CB1 and β -Arrestin1 Interface

In order to elucidate whether CB1³⁹¹⁻⁴⁰⁹ and β -arr1⁶³⁻⁷⁶ peptides are prone to interact, we acquired NMR spectra of the peptide mixture in the same conditions as for the isolated peptides. All the residues in the mixtures were unequivocally assigned (Supporting Information Tables S9–S11). As seen in the spectral regions shown in Figure 6 (see also Figures S5–S7), some cross-peaks are shifted in the spectra of the peptide mixture relative to the isolated peptides in the three examined experimental conditions. This result provides evidence that these two short peptides by themselves are able to interact each other.

In aqueous solution, some cross-peaks belonging to CB1³⁹¹⁻⁴⁰⁹ showed significant differences in the mixture relative to the isolated peptide (the most affected residues are D403 and H406; Figure 7A), whereas those of β -arr1⁶³⁻⁷⁶ were hardly affected (Figure 7A). This suggests that the interaction of these two peptides in aqueous solution requires some structural rearrangement in CB1³⁹¹⁻⁴⁰⁹, but not in β -arr1⁶³⁻⁷⁶, whose conformational equilibrium remains mainly unaffected.

However, in TFE and DPC, significant weighted NMR chemical shift differences were observed in both β -arr1⁶³⁻⁷⁶ and CB1³⁹¹⁻⁴⁰⁹ moieties when comparing the independent peptides with the mixture (Figure 7B,C). These changes are remarkable in residues D403 and H406 for CB1³⁹¹⁻⁴⁰⁹ (which are also affected in aqueous solution; Figure 7A) and E66, D67 and D69 for β -arr1⁶³⁻⁷⁶ in TFE. DPC mixtures showed weighted NMR chemical shift differences in residues R400 and K402 of CB1³⁹¹⁻⁴⁰⁹ and R65, E66, L68, D69 and L73 of β -arr1⁶³⁻⁷⁶. Table S13 summarizes the residues whose chemical shifts are affected upon interaction in each experimental condition.

These results show that short model peptides encompassing residues belonging to the putative contact region in the model of the CB1/ β -arrestin1 complex (Figure 1) are able to interact. Thus, these short sequences seem to contain enough information to recognize each other. However, how they interact seems to depend on the environment. The conformational rearrangement in CB1 is likely similar in water and in TFE, since the affected residues are essentially the same. But, upon CB1³⁹¹⁻⁴⁰⁹ interaction, β -arr1⁶³⁻⁷⁶ suffers some reorganization in the presence of TFE, but hardly change in water.

In the presence of DPC micelles, the two peptides might experience some conformational rearrangements, albeit somehow differently from those in water and TFE. These conformational changes might play a role in the CB1 β -arrestin 1 activation.

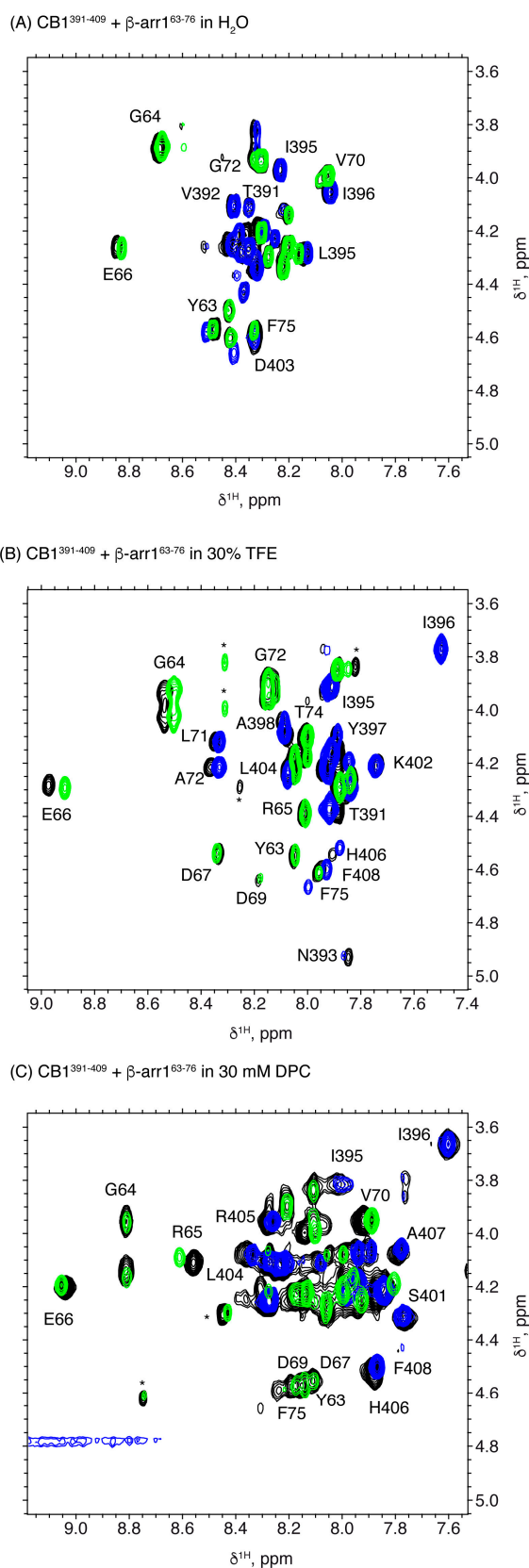


Figure 6. Overlay of selected regions of 2D $^1\text{H}, ^1\text{H}$ TOCSY spectra for CB1³⁹¹⁻⁴⁰⁹ + β -arr1⁶³⁻⁷⁶ (black contours), CB1³⁹¹⁻⁴⁰⁹ (blue contours) and β -arr1⁶³⁻⁷⁶ (green contours) in water (A), in 30 % TFE (B) and in DPC micelles (C). In all cases pH 5.5 and 25 °C.

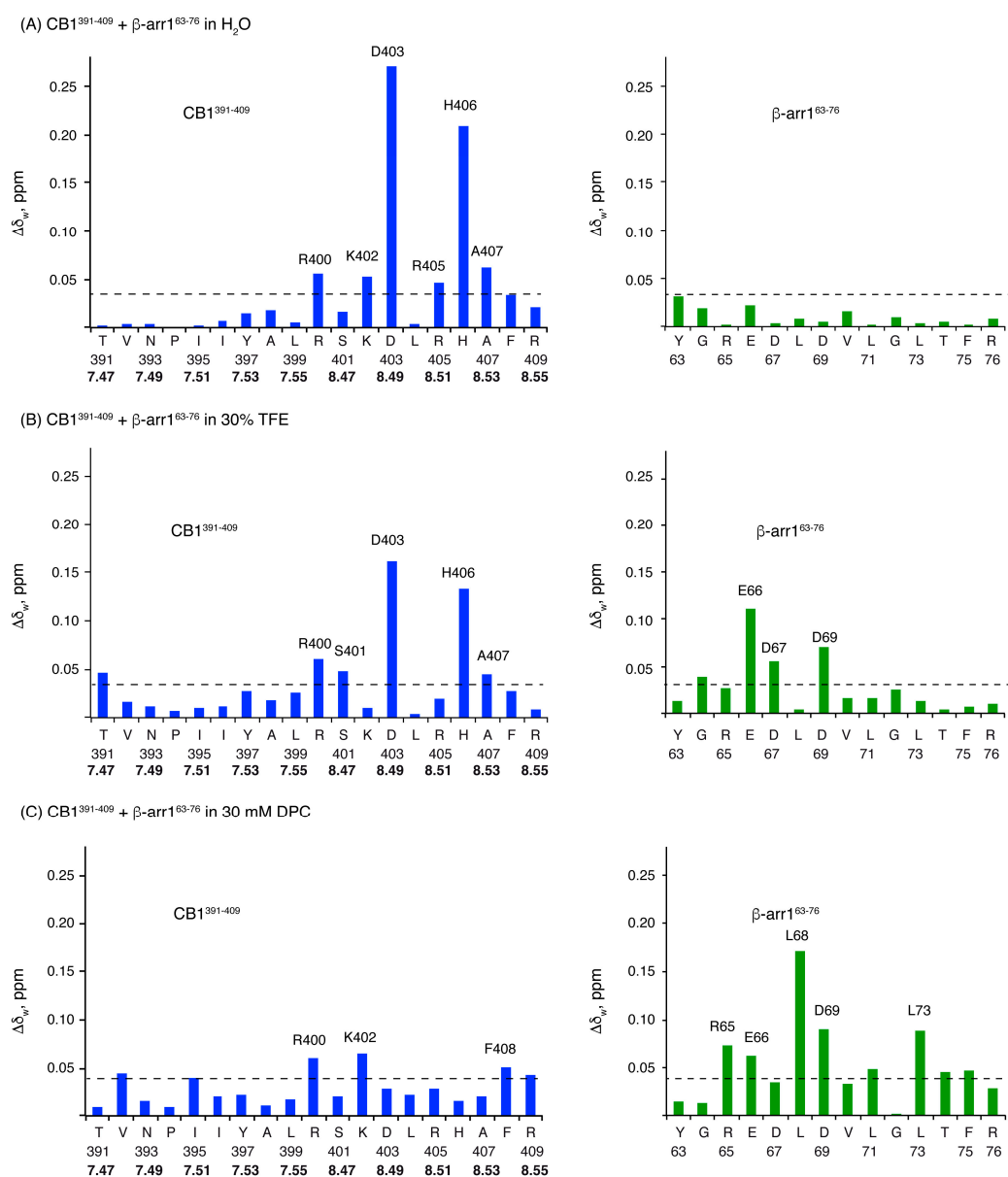


Figure 7. Weighted chemical shift differences ($\Delta\delta_w$, ppm) plotted as a function of peptide sequence for CB1³⁹¹⁻⁴⁰⁹ (blue bars) and β -arr1⁶³⁻⁷⁶ (green bars). $\Delta\delta_w$ values are calculated as $\Delta\delta_w = [(\Delta\delta_{H\alpha\text{interaction}})^2 + (\Delta\delta_{NH\alpha\text{interaction}})^2 + ((\Delta\delta_{C\alpha\text{interaction}})^2/4)]^{1/2}$, where $\Delta\delta_{H\alpha\text{interaction}}$, $\Delta\delta_{NH\alpha\text{interaction}}$ and $\Delta\delta_{C\alpha\text{interaction}}$ are the chemical shift differences of the corresponding nuclei for the free peptides and in the mixture in H₂O (A), 30% TFE (B) or 30 mM DPC (C) at pH 5.5 and 25 °C. In the case of CB1³⁹¹⁻⁴⁰⁹, the Ballesteros and Weinstein numbering is shown in bold.

As previously mentioned, structural rearrangements of the arrestin finger loop have already been observed depending on the environment, providing evidence for its necessary plasticity to couple to diverse GPCRs [51,53,55]. Table S14 displays the sequence diversity at the interface region of the GPCRs elucidated in complex with arrestins compared to CB1. This demonstrates the ability of the finger loop domain to conformationally adapt according to the interacting partner.

To visualize how the peptides contact each other and if they are reproducing the way of interaction of the full-length proteins, we proceeded to model the complexes. For that purpose, we used the Haddock-webserver introducing the structures calculated for the isolated peptides in TFE and in DPC as input. This program requires the definition of interacting residues defined as active in the docking

interface. These are the amino acids whose resonances show changes in the peptide mixture for each condition (Figure 7). Figure 8 depicts a representative model of the CB1³⁹¹⁻⁴⁰⁹/β-arr1⁶³⁻⁷⁶ complex in each condition selected from the cluster with the best Haddock docking score. These models exhibit the different rearrangement of the peptides, depending on the environment. While in DPC, β-arr1⁶³⁻⁷⁶ is almost parallel to the H8 portion of CB1³⁹¹⁻⁴⁰⁹, in TFE, β-arr1⁶³⁻⁷⁶ sits perpendicularly to both CB1³⁹¹⁻⁴⁰⁹ helical domains. Main interactions involved in the interface of the TFE complex model include hydrogen bonds between K402 and D69, H406 and E66, and the interaction formed by E66 backbone with D403 side chain (Figure 8A). The DPC complex model is mainly stabilized by hydrogen bond interactions of R400 with E66 and D69, and L68 backbone with S401 side chain (Figure 8B). In both conditions, there is also a reduction of solvent accessible surface area (ASA) upon complex formation in β-arr1 residues E66 and D69. These divergences in the peptide rearrangement, depending on the environment, could be due to the conformational plasticity of the studied region. This is in agreement with the structural diversity observed in the GPCR/arrestin finger loop interface of the reported complexes [51–55].

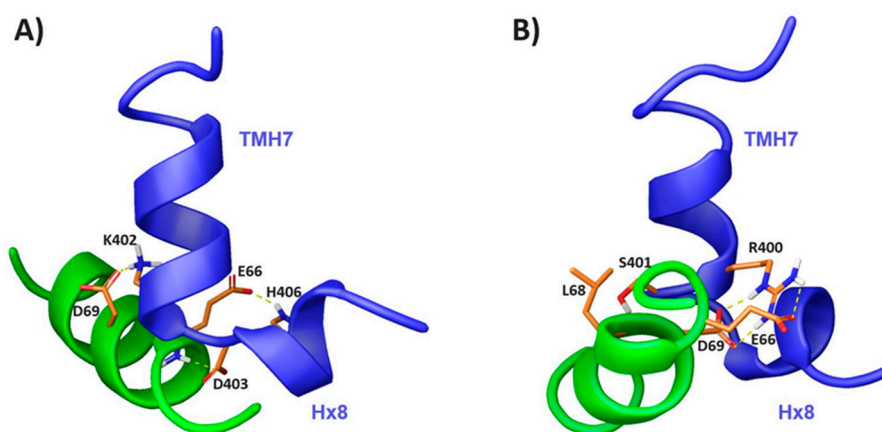


Figure 8. CB1³⁹¹⁻⁴⁰⁹/β-arr1⁶³⁻⁷⁶ complex models in TFE (A) and DPC (B). Main interacting residues are displayed in orange and yellow dashed lines represent hydrogen bonds.

It is worth noting that in the few GPCR-arrestin complexes reported thus far (none of them with CB1 receptors), residues in analogous positions of the GPCR and arrestin play a key role in their interface. For instance, residue D69 in activated β-arrestin1 was shown to directly engage with the elbow region of the β1-adrenergic receptor in a recently elucidated complex [51].

3. Materials and Methods

3.1. Chemicals and Peptides

The deuterated compounds and solvents [D₃₈]-dodecylphosphocholine (DPC) (98%), [D₃]-2,2,2-trifluoroethanol (TFE) (99%) and D₂O (99.9%) were purchased from Cambridge Isotope Laboratories (USA). Deuteration percentages are given in parentheses.

Designed peptides, with acetylated amino termini and amidated carboxylate ends, were synthesized on demand by CASLO ApS (Denmark). Solid-phase synthetic procedures along with reverse-phase HPLC purification yielded the desired peptides with the indicated purities:

- CB₁ peptide (CB1³⁹¹⁻⁴⁰⁹; Ac-TVNPIIYALRSKDLRHAFR-NH₂): HPLC: t_R = 17.2 min; 95.3% (gradient: 18-36% B in 23 min; buffer A: 0.05% TFA + 2% CH₃CN; buffer B: 0.05% TFA + 90% CH₃CN). MALDI-TOF: Theoretical MW = 2311.74; Found [M+H]⁺ = 2312.17.
- β-arrestin1 peptide (β-arr1⁶³⁻⁷⁶; Ac-YGREDLDVLGLTFR-NH₂): HPLC: t_R = 7.9 min; 95.0% (gradient: 30-44% B in 14 min; buffer A: 0.05% TFA + 2% CH₃CN; buffer B: 0.05% TFA + 90% CH₃CN). MALDI-TOF: Theoretical MW = 1694.93; Found [M+H]⁺ = 1696.22.

3.2. Peptide Numbering

The absolute sequence number of peptide residues was used throughout the article. The Ballesteros–Weinstein numbering system for GPCR amino acid residues is provided in Figure 1 to facilitate the identification of key GPCR positions [63].

3.3. CD Spectroscopy

CD spectra of the peptides were recorded using a J-815 spectropolarimeter (JASCO, Groß-Umstadt, Germany). Stock solutions of each peptide were prepared at a nominal concentration of 1 mg mL⁻¹ in milliQ-water. Samples in DPC micelles were prepared by dilution of a 30 mM DPC stock solution in milliQ-water. In both conditions, peptide final concentrations were 50 μM. Measurements were recorded at 5 °C in a quartz glass cells (Suprasil, Hellma, Müllheim, Germany) of 1 mm path length, between 260 and 190 nm at 0.1 nm intervals.

Isothermal spectra for these samples were acquired at a scan speed of 50 nm min⁻¹ with a response time of 4 s and 1 nm bandwidth. Over four scans were averaged for each sample and for the baseline of the corresponding peptide-free sample. Upon baseline correction, CD data were processed with the adaptive smoothing method integrated in the Jasco Spectra Analysis software. CD data are given in molar ellipticity units ([θ], deg cm² dmol⁻¹) for the isolated peptides and ellipticity units (θ, mdeg) for mixtures.

Estimations of the helix percentages for the free peptides were obtained from the experimental [θ] value at 222 nm ([θ]^{222nm}, deg.cm².dmol⁻¹) by applying Equation (1):

$$\% \text{ helix} = \frac{-[\theta]^{222\text{nm}} + 3000}{39000} \quad (1)$$

3.4. NMR Studies

3.4.1. Sample Preparation

Lyophilized peptides were dissolved in a final volume of 0.5 mL of solvent; that is, H₂O/D₂O (9:1 ratio by volume), pure D₂O, 30% [D₃]-TFE/70% H₂O/D₂O (9:1), and 30 mM [D₃₈]-DPC in H₂O/D₂O (9:1, *v/v*) or in pure D₂O. Final peptide concentrations were of 1.0 mM in all the NMR samples. The pH was measured using a glass micro-electrode and adjusted to 5.5 by addition of NaOD or DCl. Samples were placed in 5 mm NMR tubes and 2 μL of sodium 2,2-dimethyl-2-silapentane-5-sulfonate (DSS) were added as internal reference for ¹H chemical shifts.

3.4.2. Spectra Acquisition

A Bruker Avance-600 spectrometer (600 MHz) was used to record NMR spectra. Standard techniques were used to acquire 2D spectra: COSY (phase sensitive correlated spectroscopy), TOCSY (total correlated spectroscopy), and NOESY (nuclear Overhauser enhancement spectroscopy). Water signal suppression was achieved by presaturation or Watergate [64]. Mixing times of 60 ms were used to record the TOCSY spectra while 150 ms were used for the NOESY. ¹H-¹³C HSQC (heteronuclear single quantum coherence spectroscopy) were acquired at ¹³C natural abundance. The IUPAC-IUB recommended ¹H/¹³C chemical shift ratio was employed to indirectly referenced the ¹³C chemical shifts [65]. Depending on the experimental conditions, peptide samples were tested at 5 and/or 25 °C. Data processing was accomplished using the TOPSPIN software (Bruker Biospin, Karlsruhe, Germany).

3.4.3. Spectra Assignment

The well-established sequential methodology based on homonuclear spectra [66] was used to assign the NMR spectra of each sample. This was done using the tools provided by the NMR assignment program SPARKY (NMRFAM-Sparky version 1.4) [67]. ¹³C resonances were assigned based on the cross-peaks observed in the ¹H-¹³C-HSQC spectra. ¹H and ¹³C chemical shifts are listed in

the Supporting Tables S3–S11 and been deposited at the BioMagResBank (<http://www.bmrb.wisc.edu>) with accession codes BMRB ID: 50372-50377 and 50382-50384.

3.4.4. Estimation of Helix Populations

Helix populations were obtained from the H_{α} and $^{13}C_{\alpha}$ chemical shifts as previously described [68]. The errors in the populations estimated from the H_{α} and $^{13}C_{\alpha}$ chemical shifts are approx. 3 and 7%, respectively, assuming experimental errors of 0.01 and 0.1 ppm in the measurement of 1H and ^{13}C chemical shifts.

3.5. Structure Calculation

Structure calculations of the studied peptides were performed using the iterative procedure for automatic NOE assignment integrated in the CYANA 3.97 program [69]. The CYANA algorithm uses an iterative process having seven cycles, in which NOEs are automatically assigned by a probabilistic treatment, and structures are calculated from them. The program computes 100 conformers per cycle, minimizing the 20 structures with the lowest target functions.

The assigned chemical shifts, the NOE integrated cross-peaks (as observed in the NOESY spectra) and the φ and ψ dihedral angle restraints (obtained using TALOSn webserver [70]) were used as experimental input data for structure calculation (Table S12).

The Maestro software, integrated in the Schrödinger 2018 package (Schrödinger Inc., Portland, OR, USA), and the MOLMOL program [68] were used to visualize and examine the final ensembles of the 20 lowest target function conformers. The protein preparation wizard implemented in Maestro was used to assess their quality and ensure structural correctness.

3.6. NMR-Driven Docking

A model of the CB1/ β -arrestin1 interaction complex was built using the Haddock-webserver (<http://milou.science.uu.nl/services/HADDOCK2.2/>) [71,72]. The PDB coordinates determined herein for the solution structure of each peptide were used as input. The active residues in the docking interface were those whose NMR signals in the free peptides and in the mixture showed significant differences. These active residues guide the search for the best interacting way of the two input molecules. Haddock follows a rigid body energy minimization to cluster the complex models. In this way, the 200 complex models with lowest energy values were clustered and then refined using semiflexible docking and explicit water solvation. Representative complexes were those showing the best Haddock docking scores.

4. Conclusions

In the search of improved therapeutics targeting CB1 receptors, biased ligands are currently a major hope and challenge for avoiding undesired effects while optimizing the beneficial outcome. The design of these compounds clearly depends on an in-depth structural understanding of the GPCR-effector mechanism.

Since the G-protein interaction to CB1 has already been extensively explored [49,50], in this work, we aim to provide insights into the CB1/ β -arrestin1 interface. This arrestin isoform was chosen due to the fact that it can provoke G protein-independent activation of the ERK signaling pathway [27]. For this purpose, based on reported complexes of β -arrestin with other GPCRs, we identified a putative binding region of the β -arrestin1 finger loop in CB1. We characterized the structure of the CB1 TMH7-H8 elbow region and the β -arrestin1 finger loop, as well as their interaction using model peptides. The structural data obtained using CD and NMR studies indicated that both peptides had a slight tendency to be helical in aqueous solution, with the helical conformations being greatly stabilized in the presence of TFE and DPC micelles. It should be noted that TFE is a secondary structure enhancer, which has been shown to stabilize both helices and β -sheets [60,73] and that amphipathic structures, helical or not, seem to be favored in DPC micelles [74]. NMR characterization of CB1³⁹¹⁻⁴⁰⁹ confirmed

the formation of two distinct helical motifs orthogonally oriented mimicking their corresponding region at TMH7 and H8. Therefore, this short peptide is able to maintain, at least partially, the structure of the full-length protein. Concerning β -arr1⁶³⁻⁷⁶ finger loop model peptide, it tended to adopt helical conformations, which is in agreement with some of the reported activated β -arrestins [54–56,62], but not with others in which the finger loop is not helical [51,53]. The fact that the helix stability of the β -arr1⁶³⁻⁷⁶ finger loop is low might be related to the plasticity of this region to adopt diverse structures in order to adapt to its partner. So, this short peptide would be reproducing the structural behavior of the full-length protein.

More interestingly, as observed in the peptides mixture spectra, residues at the TMH7-H8 elbow can interact with the domain of the β -arrestin1 finger loop. This structural information is in agreement with the few previously reported structures of β -arrestins in complex with other class A GPCRs such as the rhodopsin or the β 1-adrenergic receptors [51–53,55]. Structural changes at this intracellular receptor region may suggest that the extracellular domain of the TMH1-2-7 region is involved in ligand binding of CB1 β -arrestin1 biased ligands. Therefore, this information may provide further insights into the design of novel CB1 molecules with optimized therapeutic outcomes.

In the context of the intricate GPCR signaling, β -arrestin pathway inhibition can help in elucidating specific pharmacological outcomes through other effector proteins. So far, β -arrestin blockage has been mainly accomplished through the use of siRNA-mediated knockdown or CRISPR/Cas9 methods, due to the lack of other analytical tools [75]. Our studied β -arrestin1 finger loop peptide β -arr1⁶³⁻⁷⁶ demonstrated the ability to interact with the CB1 TMH7-H8 elbow region. Therefore, this peptide could represent a useful pharmacological tool to block β -arrestin1 binding to this cannabinoid receptor under particular conditions, facilitating the study of its intriguing signaling.

In summary, our results show that short peptides encompassing the sequences of the TMH7-H8 intracellular domain and the β -arrestin1 finger loop tend to adopt the structural features of the full-length proteins, and are able to interact each other in a way that parallels the putative CB1/ β -arrestin1 interface, as deduced from other GPCR/arrestin complexes. Apart from providing structural insights into the CB1/ β -arrestin1 recognition, our findings might open a way towards the selective blocking of the β -arrestin1 pathway. Further studies using CB1³⁹¹⁻⁴⁰⁹ and β -arr1⁶³⁻⁷⁶ mutants and considering TMH6 and intracellular loops will be developed in order to fully unravel the key molecular features involved in CB₁ recognition of the finger loop domain of β -arrestin1, which would evidently also be understood if the structure of the whole CB1/ β -arrestin1 complex is determined in the future.

Supplementary Materials: Supplementary materials can be found at <http://www.mdpi.com/1422-0067/21/21/8111/s1>. Figure S1. Selected regions of the 2D ¹H, ¹H NOESY of CB1³⁹¹⁻⁴⁰⁹ in TFE and in DPC micelles. Figure S2. Selected regions of the 2D ¹H, ¹H NOESY of β -arr1⁶³⁻⁷⁶ in TFE and in DPC micelles. Figure S3. $\Delta\delta C\alpha$ conformational shifts as a function of peptide sequence for CB1³⁹¹⁻⁴⁰⁹ and β -arr1⁶³⁻⁷⁶ peptides. Figure S4. Ramachandran plots for the NMR structures of CB1³⁹¹⁻⁴⁰⁹ and β -arr1⁶³⁻⁷⁶ in 30 % TFE and in DPC micelles. Figure S5. Overlay of selected regions of 2D ¹H, ¹H TOCSY spectra for the mixture of CB1³⁹¹⁻⁴⁰⁹ plus β -arr1⁶³⁻⁷⁶, and for the isolated CB1³⁹¹⁻⁴⁰⁹ and β -arr1⁶³⁻⁷⁶ in aqueous solution at 5 oC. Figure S6. Overlay of selected regions of 2D ¹H, ¹H TOCSY spectra for the mixture of CB1³⁹¹⁻⁴⁰⁹ plus β -arr1⁶³⁻⁷⁶, and for the isolated CB1³⁹¹⁻⁴⁰⁹ and β -arr1⁶³⁻⁷⁶ in 30% TFE at 25 oC. Figure S7. Overlay of selected regions of 2D ¹H, ¹H TOCSY spectra for the mixture of CB1³⁹¹⁻⁴⁰⁹ plus β -arr1⁶³⁻⁷⁶, and for the isolated CB1³⁹¹⁻⁴⁰⁹ and β -arr1⁶³⁻⁷⁶ in DPC micelles at 25 oC. Table S1. β -arrestin1 finger loop peptide design. Table S2. CB1 TMH7-Hx8 peptide design Tables S3–S11. ¹H, and ¹³C chemical shifts of CB1³⁹¹⁻⁴⁰⁹ and β -arr1⁶³⁻⁷⁶ peptides under different experimental conditions. Table S12. Summary of structural statistics parameters for CB1³⁹¹⁻⁴⁰⁹ and β -arr1⁶³⁻⁷⁶ peptides. Table S13. CB1³⁹¹⁻⁴⁰⁹ and β -arr1⁶³⁻⁷⁶ residues whose chemical shifts are affected upon interaction. Table S14. Sequence alignment of GPCRs reported in complex with arrestins compared to CB1 at the studied TMH7-H8 region.

Author Contributions: Methodology, P.M., M.B., M.A.J.; investigation, P.M., M.B., M.A.J.; writing—original draft preparation, P.M., M.A.J.; writing—review and editing, P.M., M.B., M.A.J.; funding acquisition, M.A.J. All authors have read and agreed to the published version of the manuscript.

Funding: This research was funded by project CTQ2017-84371P (AEI/FEDER, UE). PM was a recipient of a “Juan-de-la-Cierva” post-doctoral fellowship FJCI-2016-29227. P.M. also acknowledges the “Comunidad de Madrid” program “Atraccion de Talento” 2018-T2/BMD-10819.

Acknowledgments: We acknowledge support of the publication fee by the CSIC Open Access Publication Support Initiative through its Unit of Information Resources for Research (URICI). The NMR experiments were performed in the “Manuel Rico” NMR laboratory, LMR, CSIC, a node of the Spanish Large-Scale National Facility ICTS R-LRB.

Conflicts of Interest: The authors declare no conflict of interest.

Abbreviations

AC	Adenylyl cyclase
cAMP	Cyclic adenosine monophosphate
CB1	Cannabinoid receptor type 1
CD	Circular dichroism
COSY	Phase sensitive correlated spectroscopy
DPC	Dodecylphosphocholine
FL	Finger loop
pERK1/2	Extracellular signal-regulated kinase 1/2
GIRKs	G protein-coupled inwardly-rectifying potassium channels
GPCR	G protein-coupled receptor
GRKs	G protein-coupled receptor kinases
MAPK	Mitogen-activated protein kinases
NOESY	Nuclear Overhauser enhancement spectroscopy
PI3K	Phosphatidylinositide-3-kinase
TFE	Trifluoroethanol
TMH	Transmembrane helix
TOCSY	Total correlated spectroscopy
VGCC	Voltage-gated calcium channels

References

1. Devane, W.A.; Dysarz, F.A.; Johnson, M.R.; Melvin, L.S.; Howlett, A.C. Determination and characterization of a cannabinoid receptor in rat brain. *Mol. Pharm.* **1988**, *34*, 605–613.
2. Matsuda, L.A.; Lolait, S.J.; Brownstein, M.J.; Young, A.C.; Bonner, T.I. Structure of a cannabinoid receptor and functional expression of the cloned cDNA. *Nature* **1990**, *346*, 561–564. [[CrossRef](#)] [[PubMed](#)]
3. Onaivi, E.S. Cannabinoid Receptors in Brain: Pharmacogenetics, neuropharmacology, neurotoxicology, and potential therapeutic applications. *Int. Rev. Neurobiol.* **2009**, *88*, 335–369. [[PubMed](#)]
4. Pertwee, R.G. The pharmacology of cannabinoid receptors and their ligands: An overview. *Int. J. Obes. (Lond.)* **2006**, *30*, S13–S18. [[CrossRef](#)] [[PubMed](#)]
5. Urits, I.; Borchart, M.; Hasegawa, M.; Kochanski, J.; Orhurhu, V.; Viswanath, O. An Update of Current Cannabis-Based Pharmaceuticals in Pain Medicine. *Pain* **2019**, *8*, 41–51. [[CrossRef](#)]
6. Rodrigues, R.S.; Lourenço, D.M.; Paulo, S.L.; Mateus, J.M.; Ferreira, M.F.; Mouro, F.M.; Moreira, J.B.; Ribeiro, F.F.; Sebastião, A.M.; Xapelli, S. Cannabinoid actions on neural stem cells: Implications for pathophysiology. *Molecules* **2019**, *24*, 1350. [[CrossRef](#)]
7. Billakota, S.; Devinsky, O.; Marsh, E. Cannabinoid therapy in epilepsy. *Curr. Opin. Neurol.* **2019**, *32*, 220–226. [[CrossRef](#)]
8. Hinz, B.; Ramer, R. Anti-tumour actions of cannabinoids. *Br. J. Pharm.* **2019**, *176*, 1384–1394. [[CrossRef](#)]
9. Moreno, E.; Cavic, M.; Krivokuca, A.; Casadó, V.; Canela, E. The endocannabinoid system as a target in cancer diseases: Are we there yet? *Front. Pharm.* **2019**, *10*, 339. [[CrossRef](#)]
10. Sherman, C.; Ruthirakuhan, M.; Vieira, D.; Lanctôt, K.L.; Herrmann, N. Cannabinoids for the treatment of neuropsychiatric symptoms, pain and weight loss in dementia. *Curr. Opin. Psychiatry* **2018**, *31*, 140–146. [[CrossRef](#)]
11. Poleszak, E.; Wośko, S.; Sławińska, K.; Szopa, A.; Wróbel, A.; Serefko, A. Cannabinoids in depressive disorders. *Life Sci.* **2018**, *213*, 18–24. [[CrossRef](#)] [[PubMed](#)]

12. Reddy, P.M.; Maurya, N.; Velmurugan, B.K. Medicinal Use of Synthetic Cannabinoids—A Mini Review. *Curr. Pharm. Rep.* **2019**, *5*, 1–13. [[CrossRef](#)]
13. Morales, P.; Jagerovic, N. Novel approaches and current challenges with targeting the endocannabinoid system. *Expert Opin. Drug Discov.* **2020**, *15*, 917–930. [[CrossRef](#)] [[PubMed](#)]
14. An, D.; Peigneur, S.; Hendrickx, L.A.; Tytgat, J. Targeting Cannabinoid Receptors: Current Status and Prospects of Natural Products. *Int. J. Mol. Sci.* **2020**, *21*, 5064. [[CrossRef](#)] [[PubMed](#)]
15. Brunt, T.M.; Bossong, M.G. The neuropharmacology of cannabinoid receptor ligands in central signaling pathways. *Eur. J. Neurosci.* **2020**. [[CrossRef](#)] [[PubMed](#)]
16. Laprairie, R.B.; Bagher, A.M.; Kelly, M.E.M.; Dupré, D.J.; Denovan-Wright, E.M. Type 1 cannabinoid receptor ligands display functional selectivity in a cell culture model of striatal medium spiny projection neurons. *J. Biol. Chem.* **2014**, *289*, 24845–24862. [[CrossRef](#)] [[PubMed](#)]
17. Glass, M.; Felder, C.C. Concurrent stimulation of cannabinoid CB1 and dopamine D2 receptors augments cAMP accumulation in striatal neurons: Evidence for a Gs linkage to the CB1 receptor. *J. Neurosci.* **1997**, *17*, 5327–5333. [[CrossRef](#)]
18. Finlay, D.B.; Cawston, E.E.; Grimsey, N.L.; Hunter, M.R.; Korde, A.; Vemuri, V.K.; Makriyannis, A.; Glass, M. G α s signalling of the CB1 receptor and the influence of receptor number. *Br. J. Pharm.* **2017**, *174*, 2545–2562. [[CrossRef](#)]
19. D'Antona, A.M.; Ahn, K.H.; Wang, L.; Mierke, D.F.; Lucas-Lenard, J.; Kendall, D.A. A cannabinoid receptor 1 mutation proximal to the DRY motif results in constitutive activity and reveals intramolecular interactions involved in receptor activation. *Brain Res.* **2006**, *1108*, 1–11. [[CrossRef](#)] [[PubMed](#)]
20. Abadji, V.; Lucas-Lenard, J.M.; Chin, C.N.; Kendall, D.A. Involvement of the carboxyl terminus of the third intracellular loop of the cannabinoid CB1 receptor in constitutive activation of G(s). *J. Neurochem.* **1999**, *72*, 2032–2038. [[CrossRef](#)]
21. Lauckner, J.E.; Hille, B.; Mackie, K. The cannabinoid agonist WIN55,212-2 increases intracellular calcium via CB1 receptor coupling to G(q/11) G proteins. *Proc. Natl. Acad. Sci. USA* **2005**, *102*, 19144–19149. [[CrossRef](#)]
22. Khan, S.M.; Sung, J.Y.; Hébert, T.E. G $\beta\gamma$ subunits—Different spaces, different faces. *Pharm. Res.* **2016**, *111*, 434–441. [[CrossRef](#)]
23. Howlett, A.C. International Union of Pharmacology. XXVII. Classification of Cannabinoid Receptors. *Pharm. Rev.* **2002**, *54*, 161–202. [[CrossRef](#)] [[PubMed](#)]
24. Ibsen, M.S.; Finlay, D.B.; Patel, M.; Javitch, J.A.; Glass, M.; Grimsey, N.L. Cannabinoid CB1 and CB2 Receptor-Mediated Arrestin Translocation: Species, Subtype, and Agonist-Dependence. *Front. Pharm.* **2019**, *10*, 350. [[CrossRef](#)] [[PubMed](#)]
25. Flores-Otero, J.; Ahn, K.H.; Delgado-Peraza, F.; Mackie, K.; Kendall, D.A.; Yudowski, G.A. Ligand-specific endocytic dwell times control functional selectivity of the cannabinoid receptor 1. *Nat. Commun.* **2014**, *5*, 1–11. [[CrossRef](#)] [[PubMed](#)]
26. Delgado-Peraza, F.; Ahn, K.H.; Nogueras-Ortiz, C.; Mungrue, I.N.; Mackie, K.; Kendall, D.A.; Yudowski, G.A. Mechanisms of Biased beta-Arrestin-Mediated Signaling Downstream from the Cannabinoid 1 Receptor. *Mol. Pharm.* **2016**, *89*, 618–629. [[CrossRef](#)]
27. Wouters, E.; Walraed, J.; Banister, S.D.; Stove, C.P. Insights into biased signaling at cannabinoid receptors: Synthetic cannabinoid receptor agonists. *Biochem. Pharm.* **2019**, *169*, 113623. [[CrossRef](#)] [[PubMed](#)]
28. Wisler, J.W.; DeWire, S.M.; Whalen, E.J.; Violin, J.D.; Drake, M.T.; Ahn, S.; Shenoy, S.K.; Lefkowitz, R.J. A unique mechanism of beta-blocker action: Carvedilol stimulates beta-arrestin signaling. *Proc. Natl. Acad. Sci. USA* **2007**, *104*, 16657–16662. [[CrossRef](#)]
29. Shukla, A.K.; Violin, J.D.; Whalen, E.J.; Gesty-Palmer, D.; Shenoy, S.K.; Lefkowitz, R.J. Distinct conformational changes in beta-arrestin report biased agonism at seven-transmembrane receptors. *Proc. Natl. Acad. Sci. USA* **2008**, *105*, 9988–9993. [[CrossRef](#)]
30. Khajehali, E.; Malone, D.T.; Glass, M.; Sexton, P.M.; Christopoulos, A.; Leach, K. Biased Agonism and Biased Allosteric Modulation at the CB1 Cannabinoid Receptor. *Mol. Pharm.* **2015**, *88*, 368–379. [[CrossRef](#)]
31. Li, L.; Homan, K.T.; Vishnivetskiy, S.A.; Manglik, A.; Tesmer, J.J.G.; Gurevich, V.V.; Gurevich, E.V. G Protein-coupled Receptor Kinases of the GRK4 Protein Subfamily Phosphorylate Inactive G Protein-coupled Receptors (GPCRs). *J. Biol. Chem.* **2015**, *290*, 10775–10790. [[CrossRef](#)] [[PubMed](#)]

32. Yang, J.; Williams, A.H.; Penthala, N.R.; Prather, P.L.; Crooks, P.A.; Zhan, C.G. Binding Modes and Selectivity of Cannabinoid 1 (CB1) and Cannabinoid 2 (CB2) Receptor Ligands. *ACS Chem. Neurosci.* **2020**, *30*, 3455–3463. [[CrossRef](#)] [[PubMed](#)]
33. Bian, Y.; Jing, Y.; Wang, L.; Ma, S.; Jun, J.J.; Xie, X.Q. Prediction of Orthosteric and Allosteric Regulations on Cannabinoid Receptors Using Supervised Machine Learning Classifiers. *Mol. Pharm.* **2019**, *16*, 2605–2615. [[CrossRef](#)]
34. Jenkinson, S.; Goody, S.M.G.; Bassyouni, A.; Jones, R.; Otto-Bruc, A.; Duquennoy, S.; DaSilva, J.K.; Butler, P.; Mead, A. Translation of in vitro cannabinoid 1 receptor agonist activity to in vivo pharmacodynamic endpoints. *J. Pharm. Toxicol. Methods* **2020**, *104*, 106899. [[CrossRef](#)] [[PubMed](#)]
35. Al-zoubi, R.; Morales, P.; Reggio, P.H. Structural Insights into CB1 Receptor Biased Signaling. *Int. J. Mol. Sci.* **2019**, *20*, 1837. [[CrossRef](#)] [[PubMed](#)]
36. Morales, P.; Goya, P.; Jagerovic, N. Emerging strategies targeting CB2 cannabinoid receptor: Biased agonism and allosterism. *Biochem. Pharm.* **2018**, *157*, 8–17. [[CrossRef](#)] [[PubMed](#)]
37. Kenakin, T. Functional selectivity and biased receptor signaling. *J. Pharm. Exp.* **2011**, *336*, 296–302. [[CrossRef](#)] [[PubMed](#)]
38. Kenakin, T.; Christopoulos, A. Signalling bias in new drug discovery: Detection, quantification and therapeutic impact. *Nat. Rev. Drug Discov.* **2013**, *12*, 205–216. [[CrossRef](#)]
39. Kenakin, T.; Christopoulos, A. Measurements of ligand bias and functional affinity. *Nat. Rev. Drug Discov.* **2013**, *12*, 483. [[CrossRef](#)]
40. Wisler, J.W.; Xiao, K.; Thomsen, A.R.B.; Lefkowitz, R.J. Recent developments in biased agonism. *Curr. Opin. Cell Biol.* **2014**, *27*, 18–24. [[CrossRef](#)]
41. Weis, W.I.; Kobilka, B.K. The Molecular Basis of G Protein–Coupled Receptor Activation. *Annu. Rev. Biochem.* **2018**, *87*, 897–919. [[CrossRef](#)]
42. Flock, T.; Hauser, A.S.; Lund, N.; Gloriam, D.E.; Balaji, S.; Babu, M.M. Selectivity determinants of GPCR-G protein binding. *Nature* **2017**, *545*, 1–33. [[CrossRef](#)] [[PubMed](#)]
43. Manglik, A.; Kruse, A.C. Structural Basis for G Protein–Coupled Receptor Activation. *Biochemistry* **2017**, *56*, 5628–5634. [[CrossRef](#)] [[PubMed](#)]
44. Venkatakrishnan, A.J.; Deupi, X.; Lebon, G.; Heydenreich, F.M.; Flock, T.; Miljus, T.; Balaji, S.; Bouvier, M.; Vepreintsev, D.B.; Tate, C.G.; et al. Diverse activation pathways in class A GPCRs converge near the G-protein-coupling region. *Nature* **2016**, *40*, 383–388. [[CrossRef](#)]
45. Mahoney, J.P.; Sunahara, R.K. Mechanistic insights into GPCR-G protein interactions. *Curr. Opin. Struct. Biol.* **2016**, *41*, 247–254. [[CrossRef](#)] [[PubMed](#)]
46. Hua, T.; Vemuri, K.; Pu, M.; Makriyannis, A.; Stevens, R.C.; Liu, Z. Crystal Structure of the Human Cannabinoid CB1. *Cell* **2016**, *167*, 750–762. [[CrossRef](#)]
47. Shao, Z.; Yin, J.; Chapman, K.; Grzemska, M.; Clark, L.; Wang, J.; Rosenbaum, D.M. High-resolution crystal structure of the human CB1 cannabinoid receptor. *Nature* **2016**, *540*, 602–606. [[CrossRef](#)]
48. Hua, T.; Vemuri, K.; Nikas, S.P.; Laprairie, R.B.; Wu, Y.; Qu, L.; Pu, M.; Korde, A.; Jiang, S.; Ho, J.-H.; et al. Crystal structures of agonist-bound human cannabinoid receptor CB1. *Nature* **2017**, *547*, 468–471. [[CrossRef](#)]
49. Krishna Kumar, K.; Shalev-Benami, M.; Robertson, M.J.; Hu, H.; Banister, S.D.; Hollingsworth, S.A.; Latorraca, N.R.; Kato, H.E.; Hilger, D.; Maeda, S.; et al. Structure of a Signaling Cannabinoid Receptor 1-G Protein Complex. *Cell* **2019**, *176*, 448–458.e12. [[CrossRef](#)]
50. Hua, T.; Li, X.; Wu, L.; Iliopoulos-Tsoutsouvas, C.; Wang, Y.; Wu, M.; Shen, L.; Johnston, C.A.; Nikas, S.P.; Song, F.; et al. Activation and Signaling Mechanism Revealed by Cannabinoid Receptor-Gi Complex Structures. *Cell* **2020**, *180*, 655–665.e18. [[CrossRef](#)]
51. Lee, Y.; Warne, T.; Nehmé, R.; Pandey, S.; Dwivedi-Agnihotri, H.; Chaturvedi, M.; Edwards, P.C.; García-Nafria, J.; Leslie, A.G.W.; Shukla, A.K.; et al. Molecular basis of β -arrestin coupling to formoterol-bound β 1-adrenoceptor. *Nature* **2020**, *583*, 862–866. [[CrossRef](#)]
52. Huang, W.; Masureel, M.; Qu, Q.; Janetzko, J.; Inoue, A.; Kato, H.E.; Robertson, M.J.; Nguyen, K.C.; Glenn, J.S.; Skiniotis, G.; et al. Structure of the neurotensin receptor 1 in complex with β -arrestin 1. *Nature* **2020**, *579*, 303–308. [[CrossRef](#)] [[PubMed](#)]
53. Staus, D.P.; Hu, H.; Robertson, M.J.; Kleinhenz, A.L.W.; Wingler, L.M.; Capel, W.D.; Latorraca, N.R.; Lefkowitz, R.J.; Skiniotis, G. Structure of the M2 muscarinic receptor– β -arrestin complex in a lipid nanodisc. *Nature* **2020**, *579*, 297–302. [[CrossRef](#)] [[PubMed](#)]

54. Zhou, X.E.; He, Y.; de Waal, P.W.; Gao, X.; Kang, Y.; Van Eps, N.; Yin, Y.; Pal, K.; Goswami, D.; White, T.A.; et al. Identification of Phosphorylation Codes for Arrestin Recruitment by G Protein-Coupled Receptors. *Cell* **2017**, *170*, 457–469. [\[CrossRef\]](#) [\[PubMed\]](#)
55. Kang, Y.; Zhou, X.E.; Gao, X.; He, Y.; Liu, W.; Ishchenko, A.; Barty, A.; White, T.A.; Yefanov, O.; Han, G.W.; et al. Crystal structure of rhodopsin bound to arrestin by femtosecond X-ray laser. *Nature* **2015**, *523*, 561–567. [\[CrossRef\]](#)
56. Sente, A.; Peer, R.; Srivastava, A.; Baidya, M.; Lesk, A.M.; Balaji, S.; Shukla, A.K.; Babu, M.M.; Flock, T. Molecular mechanism of modulating arrestin conformation by GPCR phosphorylation. *Nat. Struct. Mol. Biol.* **2018**, *25*, 538–545. [\[CrossRef\]](#) [\[PubMed\]](#)
57. Wilkins, M.R.; Gasteiger, E.; Bairoch, A.; Sanchez, J.C.; Williams, K.L.; Appel, R.D.; Hochstrasser, D.F. Protein identification and analysis tools in the ExpASY server. *Methods Mol. Biol.* **1999**, *112*, 531–552.
58. Lacroix, E.; Viguera, A.R.; Serrano, L. Elucidating the folding problem of α -helices: Local motifs, long-range electrostatics, ionic-strength dependence and prediction of NMR parameters. *J. Mol. Biol.* **1998**, *284*, 173–191. [\[CrossRef\]](#)
59. Chaturvedi, M.; Maharana, J.; Shukla, A.K. Terminating G-Protein Coupling: Structural Snapshots of GPCR- β -Arrestin Complexes. *Cell* **2020**, *180*, 1041–1043. [\[CrossRef\]](#)
60. Buck, M. Trifluoroethanol and colleagues: Cosolvents come of age. Recent studies with peptides and proteins. *Q. Rev. Biophys.* **1998**, *31*, 297–355. [\[CrossRef\]](#)
61. Tyukhtenko, S.; Tiburu, E.K.; Deshmukh, L.; Vinogradova, O.; Janero, D.R.; Makriyannis, A. NMR solution structure of human cannabinoid receptor-1 helix 7/8 peptide: Candidate electrostatic interactions and microdomain formation. *Biochem. Biophys. Res. Commun.* **2009**, *390*, 441–446. [\[CrossRef\]](#)
62. Elgeti, M.; Kazmin, R.; Rose, A.S.; Szczepek, M.; Hildebrand, P.W.; Bartl, F.J.; Scheerer, P.; Hofmann, K.P. The arrestin-1 finger loop interacts with two distinct conformations of active rhodopsin. *J. Biol. Chem.* **2018**, *293*, 4403–4410. [\[CrossRef\]](#) [\[PubMed\]](#)
63. Ballesteros, J.; Weinstein, H. Integrated methods for the construction of three-dimensional models and computational probing of structure-function relations in G protein-coupled receptors. In *Methods in Neurosciences*; Stuart, C.S., Ed.; Elsevier: San Diego, CA, USA, 1995; Volume 25, pp. 366–428, ISBN 9780121852955.
64. Piotto, M.; Saudek, V.; Sklenář, V. Gradient-tailored excitation for single-quantum NMR spectroscopy of aqueous solutions. *J. Biomol. Nmr* **1992**, *2*, 661–665. [\[CrossRef\]](#) [\[PubMed\]](#)
65. Markley, J.L.; Bax, A.; Arata, Y.; Hilbers, C.W.; Kaptein, R.; Sykes, B.D.; Wright, P.E.; Wüthrich, K. Recommendations for the presentation of NMR structures of proteins and nucleic acids. IUPAC-IUBMB-IUPAB inter-union task group on the standardization of data bases of protein and nucleic acid structures determined by NMR spectroscopy. *Eur. J. Biochem.* **1998**, *256*, 1–15. [\[CrossRef\]](#) [\[PubMed\]](#)
66. Wüthrich, K.; Billeter, M.; Braun, W. Polypeptide secondary structure determination by nuclear magnetic resonance observation of short proton-proton distances. *J. Mol. Biol.* **1984**, *180*, 715–740. [\[CrossRef\]](#)
67. Lee, W.; Tonelli, M.; Markley, J.L. NMRFAM-SPARKY: Enhanced software for biomolecular NMR spectroscopy. *Bioinformatics* **2015**, *31*, 1325–1327. [\[CrossRef\]](#)
68. Chaves-Arquero, B.; Pérez-Cañadillas, J.M.; Jiménez, M.A. Effect of Phosphorylation on the Structural Behaviour of Peptides Derived from the Intrinsically Disordered C-Terminal Domain of Histone H1.0. *Chem. A Eur. J.* **2020**, *26*, 5970–5981. [\[CrossRef\]](#)
69. Güntert, P. Automated NMR Structure Calculation With CYANA. In *Protein NMR Techniques*; Humana Press: Hoboken, NJ, USA, 2004; Volume 278, pp. 353–378, ISBN 1064-3745.
70. Shen, Y.; Delaglio, F.; Cornilescu, G.; Bax, A. TALOS+: A hybrid method for predicting protein backbone torsion angles from NMR chemical shifts. *J. Biomol. Nmr* **2009**, *44*, 213–223. [\[CrossRef\]](#)
71. Van Zundert, G.C.P.; Rodrigues, J.P.G.L.M.; Trellet, M.; Schmitz, C.; Kastritis, P.L.; Karaca, E.; Melquiond, A.S.J.; Van Dijk, M.; De Vries, S.J.; Bonvin, A.M.J.J. The HADDOCK2.2 Web Server: User-Friendly Integrative Modeling of Biomolecular Complexes. *J. Mol. Biol.* **2016**, *428*, 720–725. [\[CrossRef\]](#)
72. Dominguez, C.; Boelens, R.; Bonvin, A.M.J.J. HADDOCK: A protein-protein docking approach based on biochemical or biophysical information. *J. Am. Chem. Soc.* **2003**, *125*, 1731–1737. [\[CrossRef\]](#)
73. Roccatano, D.; Colombo, G.; Fioroni, M.; Mark, A.E. Mechanism by which 2,2,2-trifluoroethanol/water mixtures stabilize secondary-structure formation in peptides: A molecular dynamics study. *Proc. Natl. Acad. Sci. USA* **2002**, *99*, 12179–12184. [\[CrossRef\]](#)

74. Zamora-Carreras, H.; Maestro, B.; Strandberg, E.; Ulrich, A.S.; Sanz, J.M.; Jiménez, M.Á. Micelle-triggered β -hairpin to α -helix transition in a 14-residue peptide from a choline-binding repeat of the pneumococcal autolysin LytA. *Chem. A Eur. J.* **2015**, *21*, 8076–8089. [[CrossRef](#)] [[PubMed](#)]
75. Luttrell, L.M.; Wang, J.; Plouffe, B.; Smith, J.S.; Yamani, L.; Kaur, S.; Jean-Charles, P.Y.; Gauthier, C.; Lee, M.H.; Pani, B.; et al. Manifold roles of β -arrestins in GPCR signaling elucidated with siRNA and CRISPR/Cas9. *Sci. Signal.* **2018**, *11*, eaat7650. [[CrossRef](#)]

Publisher’s Note: MDPI stays neutral with regard to jurisdictional claims in published maps and institutional affiliations.



© 2020 by the authors. Licensee MDPI, Basel, Switzerland. This article is an open access article distributed under the terms and conditions of the Creative Commons Attribution (CC BY) license (<http://creativecommons.org/licenses/by/4.0/>).